A nonparametric quantification of neural response field structures

Marina Brozović and Richard A. Andersen

Division of Biology, California Institute of Technology, Pasadena, California, USA

Correspondence and request for reprints to Dr Marina Brozović, California Institute of Technology, Division of Biology, 1200 E. California Blvd., Mail Code 216-76, Pasadena, CA 91125, USA
Tel: + 1 626 395 8337; fax: + 1 626 795 2397; e-mail: brozovic@vis.caltech.edu

Sponsorship: This work was supported by the James G. Boswell Foundation, the Sloan-Swartz Center for Theoretical Neurobiology and the National Eye Institute.

Received 30 March 2006; accepted 3 April 2006

The response fields of higher cortical neurons are usually approximated with smooth mathematical functions for the purpose of population parameterization or theoretical modeling. We used instead two nonparametric methods (principal component analysis and independent component analysis), which provided a basis for the response field clustering. Although both methods performed satisfactorily, the principal component analysis space is more straightforward to calculate. It also gave a clear preference toward the smallest number of functional response field classes. Clustering was performed with both K-means and superparamagnetic clustering algorithms with similar results. We also show that the shapes of the eigenvectors remain consistent regardless of the response field data sets size. This finding reflects the fact that the response fields were generated by the same neural network and encode the same underlying process. *NeuroReport* 17:963–967 © 2006 Lippincott Williams & Wilkins.

Keywords: independent component analysis, parietal cortex, principal component analysis, shapes of the response fields

Introduction

The present study addresses parameterization of the response field (RF) shapes for higher cortical neurons [e.g. posterior parietal cortex (PPC)]. A static description of the RF is typically defined as a two-dimensional (2D) map of the average firing rate in Hz with respect to the spatial position of the stimulus or the action that the neuron encodes. Experimentally, the RFs of the neurons in the PPC are frequently mapped out in tasks in which trained rhesus monkeys perform saccadic or reach movements with respect to a grid of visual or auditory targets [1–5]. Furthermore, the intensity of the RF is often modulated by the position of the 'effector' (e.g. eye position, head position, hand position, etc. [6–8]).

The RFs of parietal (and other) neurons are in most analyses fitted to some mathematical function. For example, neuronal responses in the lateral intraparietal cortex, a subdivision of PPC, have been approximated by Cartesian 2D Gaussian functions [9,10]. The RFs of the neighboring middle temporal area neurons are often modeled by elliptical functions [11,12], whereas the responses of the neurons in the motor cortex are most frequently represented by cosine functions [13]. In many experiments, the RFs are undersampled by the limited number of targets (sensory or motor) that are used to map the RFs. Although some of neurons indeed have very smooth RFs, others have RFs with more complex structures [13–15].

A motivation for this study was to establish a method that would give a quantitative measure of the RFs shapes without first parameterizing them with some mathematical function. We decided to use techniques already developed in face recognition studies such as principal component analysis (PCA) and independent component analysis (ICA). Recently, PCA was used to express the variability of the RFs developed in a neural network [16]. Our analysis also uses a neural network to provide a population of RFs. The advantage of using a neural network for this particular study is that the RFs can be mapped at a much higher resolution and for more parameters than is typically obtained in physiological recording experiments.

Methods

Neural network

Although the goal of this paper is to concentrate on the RF shape analysis, a brief overview of the network architecture and its training is presented. The network was trained to perform the well-studied coordinate transformation in which information on the position of an auditory target, initially represented in the head-centered reference frame, is converted into an eye-centered reference frame [3,17,18]. A three-layer perceptron network [7,19] was constructed from an input, an output and a hidden layer. The input layer contained 2D map of Gaussian units encoding sound in the head, as well as 2D map of sigmoidal units encoding eye position in the head. The output layer had 2D map of Gaussian units encoding the sound in the eye. Forty units exist performing coordinate transformations in the

Copyright © Lippincott Williams & Wilkins. Unauthorized reproduction of this article is prohibited.

hidden layer using noise-modulated nonlinear transfer functions [20].

The network training was performed using the back-propagation algorithm. The performance was tested with an input of 8×8 uniformly distributed (from -35° to $+35^\circ$) target sound positions (head-centered reference frame) and a single eye position. The same set of test data was used to map RFs that developed in the hidden units. Twenty-three out of 40 units had their activation values greater than 25% of the maximum activation value observed among the hidden units. These were the units that we deemed 'significantly active' and suitable for the shape analysis. In order to increase the statistics of the active units, we ran the network five more times with different initialization parameters. The RFs of the hidden units were mapped in the same way, and only the ones with $>25\%$ activation were used. In summary, the network training was executed six times, which resulted in 119 out of 240 units being kept for further analysis.

Response field shapes analysis

The RFs encode different parts of the stimulus space from unit to unit, and they have different shapes. The 119 RFs were normalized with respect to their maximum firing rate. The RFs from the model were combined into a measurement matrix $[R_1\ R_2\ \ldots\ R_{119}]$, where each of the 119 columns had a length of $8 \times 8 = 64$ data points.

The PCA was used in format described in [21]. Mathematically, the PCA calculates the eigenvectors of the RFs covariance matrix. The eigenvectors capture the variability of the shapes in the set in its most condensed form. The PCA basis space consists of linearly decorrelated eigenvectors. The ICA is a powerful technique for finding a set of statistically minimally dependent basis vectors in multivariate data. The ICA was implemented via the InfoMax algorithm [22] in two architectures as described in [23]. The InfoMax parameters for this analysis were: a block size of 10 and a learning rate 0.001. It trained after several hundred epochs. The ICA architecture I was performed on the basis of the first six (and four) PCA basis vectors that encoded 96% (and 93%) of the RFs variance. For the ICA architecture II, the ICA was applied onto the RF projection coefficients for the first six (and four) PCA basis vectors. For the ICA architecture I, the basis vectors are statistically independent, but the projection coefficients of the RFs onto that basis set are not. For the ICA architecture II, as ICA is applied onto the PCA coefficients, it leads to statistically independent ICA basis projection coefficients.

We had three possible basis spaces for clustering the RFs into classes. The clustering gave a better understanding of the types of the RFs and how they tile the stimulus space. The choice of the basis space was quantified with respect to cluster separation in the particular space. The standard K-means clustering algorithm (Matlab) was applied in four-dimensional and six-dimensional basis spaces for the various numbers of clusters (Tables 1 and 2). The 'silhouette' function in Matlab provided a measure of the clusters separation. The silhouette values range from $+1$ to -1; $+1$ denote clear cluster assignment and -1 marks points with questionable cluster assignment. A successful clustering has mean silhouette value greater than 0.6 for all clusters. The metric used in both K-means and silhouette was squared Euclidean distance (cosine metrics gave similar, or worse, results). The results of K-means clustering were compared with the superparamagnetic clustering (spc) [24,25], which has the number of clusters left as a free parameter.

Table 1 K-means cluster separation expressed via silhouette value

Clusters	PCA	ICA I	ICA II
3	0.45	0.50	0.29
4	0.56	0.54	0.32
5	0.60	0.62	0.37
6	0.57	0.60	0.42
7	0.53	0.57	0.48
8	0.53	0.54	0.53

The clustering was performed in a six-dimensional basis space. The distance metric used in K-means and silhouette is squared Euclidean. Clusters are well separated for silhouette >0.6.
PCA, principal component analysis; ICA, independent component analysis.

Table 2 K-means cluster separation expressed via silhouette value

Clusters	PCA	ICA I	ICA II
3	0.47	0.53	0.4l
4	0.58	0.57	0.50
5	0.63	0.66	0.57
6	0.60	0.64	0.6l
7	0.59	0.6l	0.62
8	0.56	0.60	0.63

The clustering was performed in a four-dimensional basis space. The distance metric is the same as in Table l.
PCA, principal component analysis; ICA, independent component analysis.

The last part of the analysis examines whether the size of the data set affects the shapes of the basis vectors. This is performed by calculating eigenvectors as the number of RFs decreases by dropping the number of network runs to five, four and three (the analysis so far was performed on the basis of all six network initializations).

Results

Figure 1 shows six basis vectors for PCA (96% variance), ICA architecture I and ICA architecture II. The number of units in the data set was on the basis of six network runs and 119 out of 240 hidden units were used to calculate the eigenvectors. The cumulative sum of the PCA eigenvalues increases with each additional PCA eigen-RF-vector: 0.36, 0.69, 0.88, 0.93, 0.95 and 0.96 for the first six vectors. The ICA InfoMax algorithm then converts these six eigenvectors into two other basis sets depending on the architecture. When discussed in the face recognition literature, it is usually stated that the PCA and ICA II basis vectors encode more global features of the face, whereas ICA I vectors encode more localized features (recognition by parts).

Tables 1 and 2 show K-means clustering of the projection coefficients from 119 RFs in PCA, ICA I and ICA II basis spaces (four and six dimensions). The K-means is considered successful if the mean cluster separation (across all clusters) is greater than 0.6. The tables show that the clustering in four-dimensional space has better cluster separation than the clustering in six dimensions. The RFs are assigned to the same clusters in both four-PCA and six-PCA dimensional spaces as their projection coefficients vary very little in fifth and sixth dimensions. These eigenvectors only add 3% of the information on the variance of the RFs.

Copyright © Lippincott Williams & Wilkins. Unauthorized reproduction of this article is prohibited.

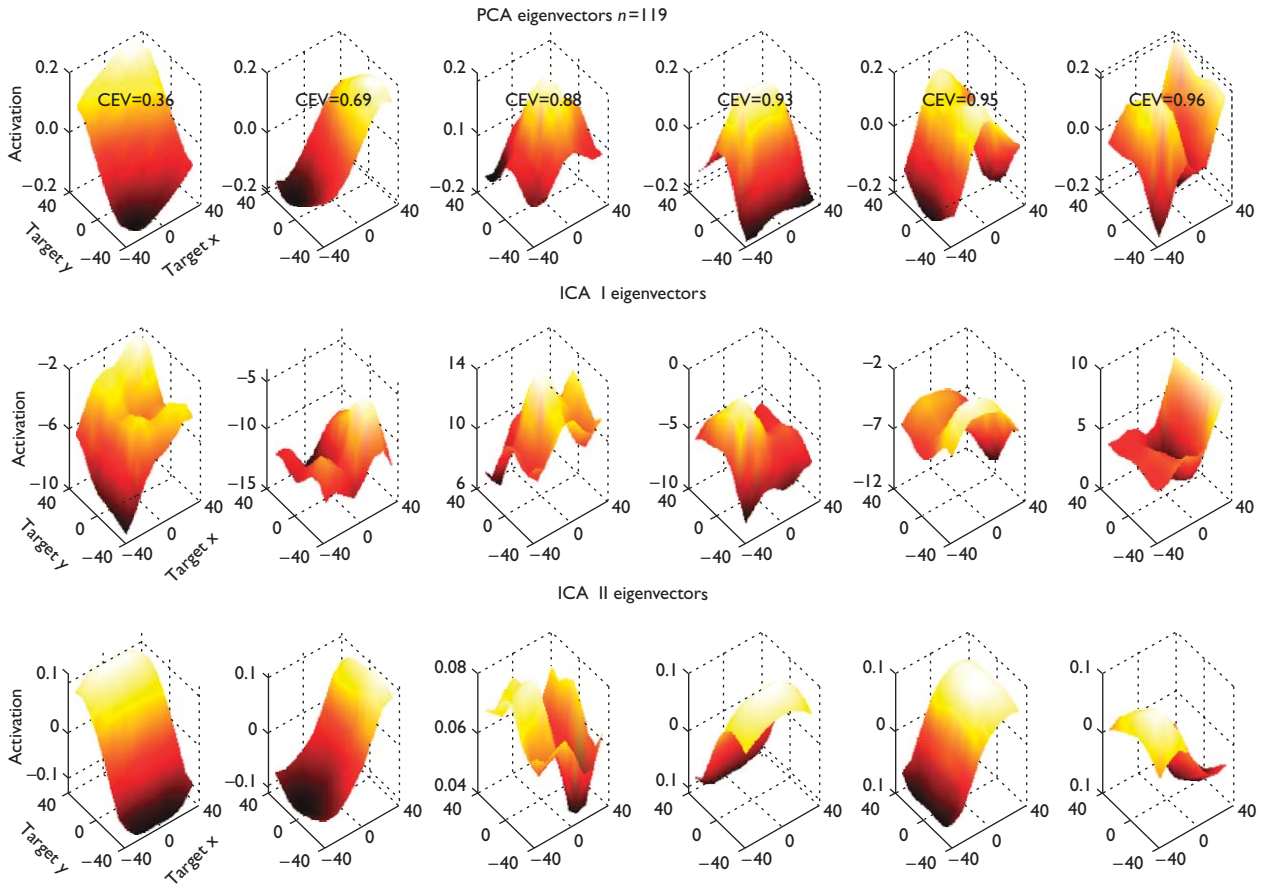

Fig. 1 Six leading eigen-response field-vectors based on n=119 units data set. First row shows principal component analysis (PCA) eigenvectors with their CEV (cumulative sum of eigenvalues). Second row represents independent component analysis (ICA) I basis vectors. Third row shows ICA II basis vectors.

The question still remains regarding what is the best basis set for the clustering? Each basis set resulted in different RF classification. PCA works best for five clusters. ICA I works well for five and six clusters. ICA II has preference toward higher numbers of clusters (7 or 8). Just on the basis of the silhouette values, there is no clear winner on the choice of the basis set among the three methods. We give a slight preference to PCA as the basis space which separates the data into five well defined classes. This is convenient in terms of visualizing what each RF category represents. When PCA and ICA I coefficients are clustered into five clusters, the classes are: top, bottom, left, right and center (Fig. 2). For 89% (106/119) of RFs the cluster assignment is the same in both basis spaces. The result of the K-means clustering in the PCA space can also be described as 31% of RFs are central and 69% RFs are peripheral (top + bottom + left + right).

The classification description becomes harder to describe as we move toward higher numbers of clusters. When the PCA coefficients are clustered in six classes, the categories top, bottom, left and right remain the same, whereas the central category splits into symmetrical central fields and irregular central fields. For the ICA I, the sixth category becomes bottom-left fields.

The K-means results are compared with the clusters obtained using the spc in four-dimensional PCA eigen-RF-space. The algorithm placed 112 (out of 119) units in the five categories. The two clustering methods had 86% of the RFs assigned to the same class.

Fig. 2 The K-means clustering sorted the hidden units according to their projections onto the first four eigen-response field (RF)-shapes. The general groups of the RFs are: top, bottom, left, right and center with respect to the head-centered stimuli space.

Figure 3 shows the average response field (RF_{AV}) and four leading PCA eigenvectors calculated on the basis of a different number of network runs. The three rows in Fig. 3 are results for the five, four and three network runs, respectively. Each RF_{AV} reflects the overall coverage of the 2D stimuli space and it remains the same whether it is calculated on the basis of 108 units (five network runs), 87 units (four network runs) or 65 units (three network runs). The stimuli space is always tiled so that the central region of the space is slightly better represented than the periphery. The shapes of the eigenvectors as well as their cumulative sum of eigenvalues also remain consistent.

Copyright © Lippincott Williams & Wilkins. Unauthorized reproduction of this article is prohibited.

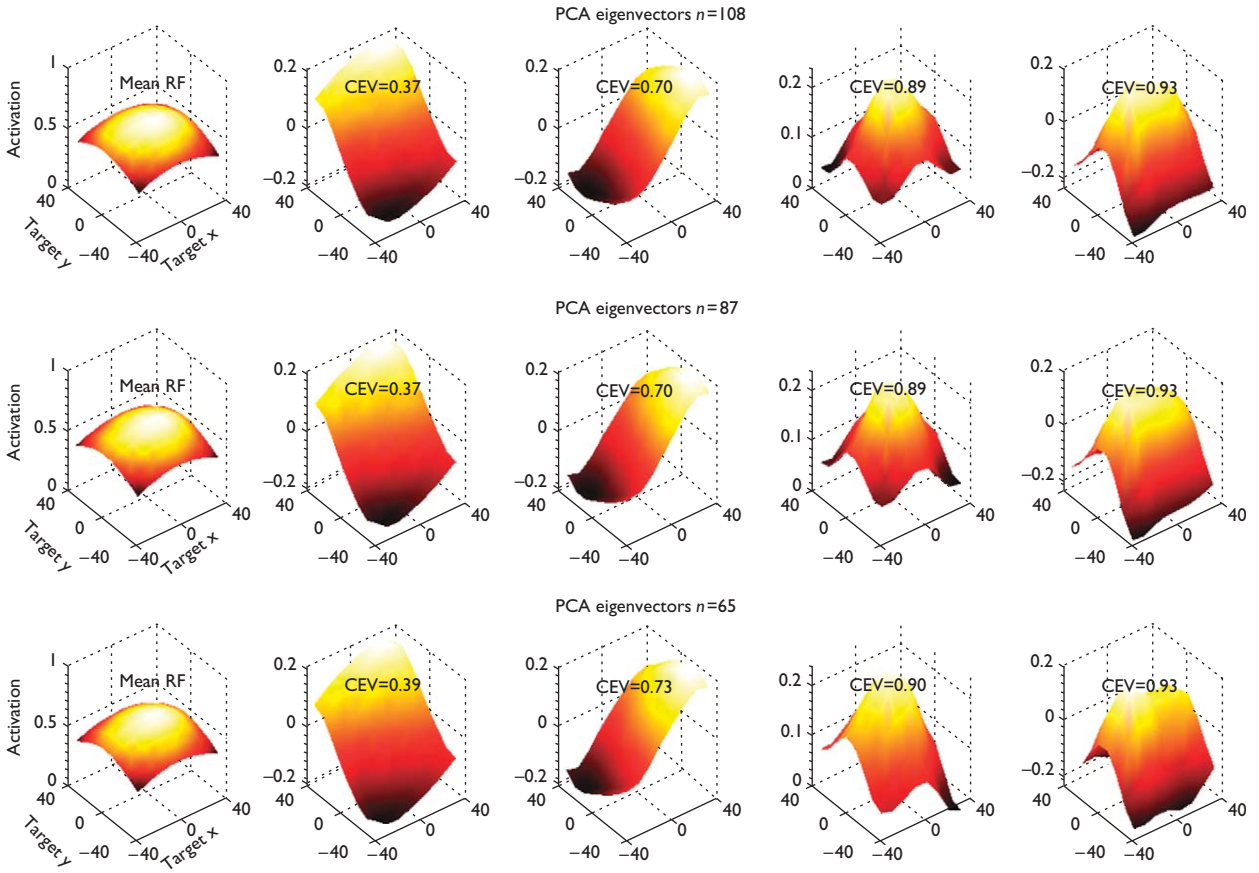

Fig. 3 The rows show the average response fields (RFs) and the first four principal component analysis (PCA) eigenvectors calculated on the basis of five, four and three network runs. *n* denotes how many hidden units were selected for the RF_{AV} and the eigenvector calculation (*n*=108, 87 and 65, respectively). CEV is the cumulative sum of eigenvalues.

Discussion

As stated in the introduction, many experiments have shown that when the neuronal responses are probed with a finer resolution of the sensory/motor targets, the RF shapes can vary substantially from cell to cell. Instead of fitting the RFs with various mathematical functions, we proposed that the RFs need to be analyzed in their original format.

The basic idea is to compress a variety of the neuronal RFs in the data into a small number of eigen-RF-shapes using several face recognition techniques. In face recognition, the performance of the PCA, ICA I and ICA II is measured by how many correct 'recognitions' there are when the new face image is presented. In [23] it was shown that both the choice of method, as well as the type of distance metrics (squared Euclidean, cosine, city-block) depends on the nature of the task (e.g. face identification vs. recognizing facial actions). In our study, the choice of the optimal basis set was tested by grouping the RFs into clusters and measuring in which basis space the clusters have best separation, thus defining the RF classes. Although it was difficult to pick one basis space over the other, we favored the PCA space as the most straightforward to calculate and interpret. It also had clear preference toward the smallest number of the RF clusters, and each cluster had an easy functional description (peripheral and central fields). The spc algorithm has an advantage over the K-means clustering because no a priori assumption on the number of clusters is needed.

An important consideration for neural recording studies is whether the shapes of the basis vectors change as more and more neurons are included in the study. We show in Fig. 3 that if the additional RFs are produced by the same neural mechanism, then their 'cumulative' eigenvectors should continue to look the same. This is said with the assumption that some minimal data set is already achieved, which can be observed in a uniform coverage of the stimulus space in RF_{AV}. A further extension of this analysis may be a direct comparison between the first few eigenvectors in a real neurons data set and the eigenvectors from a theoretical model.

Conclusion

This analysis presents an objective approach for analyzing the shapes of the RFs in higher cortical areas. The variability of RF shapes in the data set can be expressed by finding the basis-RF-set. The categories of the RF shapes may be defined based on the projection coefficients which are calculated by multiplying each RF vector by the first few eigenvectors. We also show that as the RFs shapes reflect the underlying

Copyright © Lippincott Williams & Wilkins. Unauthorized reproduction of this article is prohibited.

process that the network encodes, there exists a unique set of eigenvectors that describes its RF set.

Acknowledgments

The authors would like to thank the generous support of the James G. Boswell Foundation, the Sloan-Swartz Center for Theoretical Neurobiology and the National Eye Institute. We thank Viktor Shcherbatyuk for computer assistance and Tessa Yao for administrative assistance.

References

1. Barash S, Bracewell RM, Fogassi L, Gnadt JW, Andersen RA. Saccade-related activity in the lateral intraparietal area. I. Temporal properties; comparison with area 7a. *J Neurophysiol* 1991; **3**:1095–1108.
2. Barash S, Bracewell RM, Fogassi L, Gnadt JW, Andersen RA. Saccade-related activity in the lateral interparietal area. II. Spatial properties. *J Neurophysiol* 1991; **6**:1109–1124.
3. Grunewald A, Linden JF and Andersen RA. Responses to auditory stimuli in macaque lateral interparietal area. *J Neurophysiol* 1999; **82**: 330–342.
4. Batista AP, Buneo CA, Snyder LH, Andersen RA. Reach plans in eye-centered coordinates. *Science* 1999; **285**:257–260.
5. Buneo CA, Jarvis MR, Batista AP, Andersen RA. Direct visuomotor transformations for reaching. *Nature* 2002; **416**:632–636.
6. Andersen RA and Mountcastle VB. The influence of the angle of gaze upon the excitability of light-sensitive neurons of the posterior parietal cortex. *J Neurosci* 1983; **3**:532–548.
7. Zipser D and Andersen RA. A backpropagation programmed network that simulates response properties of a subset of posterior parietal neurons. *Nature* 1988; **331**:679–684.
8. Brotchie PR, Andersen RA, Snyder LH, Goodman SJ. Head position signals used by parietal neurons to encode locations of visual stimuli. *Nature* 1995; **375**:232–235.
9. Platt ML and Glimcher PW. Response fields of intraparietal neurons quantified with multiple saccadic targets. *Exp Brain Res* 1998; **121**:65–75.
10. Gnadt JW and Breznen B. Statistical analysis of the information content in the activity of cortical neurons. *Vis Res* 1996; **36**:3525–3537.
11. Perrone JA and Thiele A. Speed skills: measuring the visual speed analyzing properties of primate MT neurons. *Nat Neurosci* 2001; **4**: 526–532.
12. Pack CP, Born RT, Livingstone MS. Two-dimensional substructure of stereo and motion interactions in macaque visual cortex. *Neuron* 2003; **37**:525–535.
13. Amirikain B, Georgopulos AP. Directional tuning profiles of motor cortical cells. *Neurosci Res* 2000; **36**:73–79.
14. Ben Hamed S, Duhamel JR, Bremmer F, Graf W. Representation of the visual field in the lateral intraparietal area of macaque monkeys: a quantitative receptive field analysis. *Exp Brain Res* 2001; **140**:127–144.
15. Schlack A, Sterbing-D'Angelo SJ, Hartung K, Hoffmann KP, Bremmer F. Multisensory space representations in the macaque ventral intraparietal area. *J Neurosci* 2005; **25**:4616–4625.
16. Smith MA, Crawford JD. Distributed population mechanism for 3-D oculomotor reference frame transformation. *J Neurophysiol* 2005; **93**: 1742–1761.
17. Groh JM, Trause AS, Underhill AM, Clark KR, Inati S. Eye position influences auditory responses in primate inferior colliculus. *Neuron* 2001; **29**:509–518.
18. Jay MF, Sparks DL. Auditory receptive fields in primate superior colliculus shift with changes in eye positions. *Nature* 1984; **309**:345–347.
19. XingJ, Andersen RA. Models of the posterior parietal cortex which perform multimodal integration and represent space in several coordinate frames. *J Cogn Neurosci* 2000; **12**:601–614.
20. Chance FS, Abbott LF, Reyes AD. Gain modulation from background synaptic input. *Neuron* 2002; **35**:773–782.
21. Turk M, Pentland A. Eigenfaces for recognition. *J. Cogn Neurosci* 1991; **3**:71–86.
22. Bell AJ, Sejnowski TJ. The 'independent components' of natural scenes are edge filters. *Vis Res* 1997; **37**:3327–3338.
23. Draper BA, Baek K, Bartlett MS, Beveridge JR. Recognizing faces via PCA and ICA. *Comput Vis Image Understanding* 2003; **91**:115–137.
24. Blatt M, Wesemann S, Domany E. Super-paramagnetic clustering of data. *Phys Rev Lett* 1996; **76**:3251–3254.
25. Quiroga RQ, Nadasdy Z, Ben-Shaul Y. Unsupervised spike detection and sorting with wavelets and superparamagnetic clustering. *Neural Comput* 2004; **16**:1661–1687.

Copyright © Lippincott Williams & Wilkins. Unauthorized reproduction of this article is prohibited.